2006

Unusual kinetic and structural properties control rapid assembly and turnover of actin in the parasite Toxoplasma gondii

Nivedita Sahoo
Washington University School of Medicine in St. Louis
Wandy Beatty
Washington University School of Medicine in St. Louis
John Heuser
Washington University School of Medicine in St. Louis
David Sept
Washington University in St Louis
L. David Sibley
Washington University School of Medicine in St. Louis

Molecular Biology of the Cell
Vol. 17, 895–906, February 2006

Unusual Kinetic and Structural Properties Control Rapid Assembly and Turnover of Actin in the Parasite *Toxoplasma gondii*[D]

Nivedita Sahoo,* Wandy Beatty,* John Heuser,† David Sept,‡ and L. David Sibley*

*Department of Molecular Microbiology, Center for Infectious Diseases and †Department of Cell Biology and Physiology, Washington University School of Medicine, St. Louis, MO 63110; and ‡Department of Biomedical Engineering, Center for Computational Biology, Washington University, St. Louis, MO 63130

Submitted June 8, 2005; Revised October 3, 2005; Accepted November 18, 2005
Monitoring Editor: David Drubin

***Toxoplasma* is a protozoan parasite in the phylum Apicomplexa, which contains a number of medically important parasites that rely on a highly unusual form of motility termed gliding to actively penetrate their host cells. Parasite actin filaments regulate gliding motility, yet paradoxically filamentous actin is rarely detected in these parasites. To investigate the kinetics of this unusual parasite actin, we expressed TgACT1 in baculovirus and purified it to homogeneity. Biochemical analysis showed that *Toxoplasma* actin (TgACT1) rapidly polymerized into filaments at a critical concentration that was 3–4-fold lower than conventional actins, yet it failed to copolymerize with mammalian actin. Electron microscopic analysis revealed that TgACT1 filaments were 10 times shorter and less stable than rabbit actin. Phylogenetic comparison of actins revealed a limited number of apicomplexan-specific residues that likely govern the unusual behavior of parasite actin. Molecular modeling identified several key alterations that affect interactions between monomers and that are predicted to destabilize filaments. Our findings suggest that conserved molecular differences in parasite actin favor rapid cycles of assembly and disassembly that govern the unusual form of gliding motility utilized by apicomplexans.**

INTRODUCTION

Toxoplasma gondii belongs to the phylum Apicomplexa, which includes other medically important parasites such as *Plasmodium* (malaria) and *Cryptosporidium* (an agent of waterborne diarrhea). Apicomplexans are unified by their apical specializations that enable them to actively invade a variety of cell types (Morrissette and Sibley, 2002). *T. gondii* is an opportunistic pathogen that is capable of infecting all types of nucleated cells from warm-blooded vertebrates. The parasite normally causes infection by the oral route, through ingestion of contaminated food or water (Mead *et al.*, 1999). After initial entry across the gut, the parasite navigates through complex tissues to reach sites where is causes pathology, such as the CNS, retina, and placenta (Barragan and Sibley, 2003). Because of the ease of experimental manipulation, excellent genetics, and animal models, *T. gondii* provides a model for investigating the unique biology of this diverse group of parasites.

This article was published online ahead of print in *MBC in Press* (http://www.molbiolcell.org/cgi/doi/10.1091/mbc.E05–06–0512) on November 30, 2005.

[D] The online version of this article contains supplemental material at *MBC Online* (http://www.molbiolcell.org).

Address correspondence to: David Sibley (sibley@borcim.wustl.edu).

Abbreviations used: TgACT1, *Toxoplasma* actin; Cyt, cytochalasin; EM, electron microscopy; F-actin, filamentous actin; G-actin, globular actin; JAS, jasplakinolide.

Apicomplexans are obligate intracellular parasites that rely on an unusual form of motility called gliding, which is responsible for the active invasion of their host cells (Sibley, 2004). Unlike phagocytic uptake, host cell invasion by apicomplexans occurs by active penetration of host cells. Molecular genetic studies have conclusively demonstrated that filamentous actin in the parasite is essential for gliding motility and cellular invasion (Dobrowolski and Sibley, 1996). Motility is facilitated by cell surface adhesins that bind externally to the substratum, extend across the parasite plasma membrane, and link internally to the parasite's cytoskeleton (Sultan *et al.*, 1997; Buscaglia *et al.*, 2003; Jewett and Sibley, 2003). Translocation of these parasite surface adhesins from the apex of the parasite to its posterior end drives forward movement. Gliding is regulated by the availability of actin filaments (Wetzel *et al.*, 2003) and depends on a small myosin called TgMyoA (Meissner *et al.*, 2002).

In eukaryotic cells, actin exists in two states, a globular form called G-actin that is generally bound to sequestering proteins and a polymerized form called F-actin that forms filamentous networks (Pollard *et al.*, 2000). Actin is capable of self-polymerization by the formation of head-to-tail dimers that assemble into filaments consisting of two parallel strands interwoven in a right-handed helical spiral (Pollard *et al.*, 2000). Actin in *T. gondii* is encoded by a single-copy gene with 93.1% identity to *Plasmodium falciparum* and 83% to vertebrate actin (Dobrowolski *et al.*, 1997). Despite a requirement for F-actin in parasite motility, filaments are not readily detected in the parasite, where most of the actin (~97%) fails to sediment at 100,000 × *g* (Dobrowolski *et al.*, 1997; Wetzel *et al.*, 2003). Additionally, actin filaments are

not readily detected in *T. gondii* by phalloidin staining (Dobrowolski *et al.*, 1997) or transmission electron microscopy (EM; Shaw and Tilney, 1999). However, rapid freeze-etch EM of parasite cells caught in the act of gliding reveals the presence of short, unbranched actin filaments beneath the parasite plasma membrane (Wetzel *et al.*, 2003).

Gliding motility by *T. gondii* normally propels the parasite across the substrate at a rate of ~1 μm/s (Håkansson *et al.*, 1999). Gliding motility is exquisitely sensitive to agents that affect actin polymerization. Motility is blocked by Cytochalasin D (CytD; Dobrowolski and Sibley, 1996), which inhibits actin polymerization and by the actin-stabilizing drug jasplakinolide (JAS; Poupel and Tardieux, 1999; Shaw and Tilney, 1999). Importantly, JAS-treated parasites are hyperkinetic but lack normal directional control because of the inappropriate assembly of actin filaments in the parasite (Wetzel *et al.*, 2003). Collectively, these findings indicate that polymerization of actin filaments normally coordinates both the directionality and initiation of movement and that the abundance of F-actin is rate limiting for motility. However, the control of actin polymerization in apicomplexans remains poorly understood, despite a wealth of knowledge in other model systems (Pollard and Borisy, 2003).

Several recent reports on malaria actin shed some light on the nature of actin in parasites. Extraction of *P. falciparum* merozoites revealed that the majority of actin failed to sediment in high salt (equivalent to F-buffer) when centrifuged at 100,000 × *g* (Schmitz *et al.*, 2005), similar to reports of the behavior of actin in *T. gondii* (Dobrowolski *et al.*, 1997; Poupel and Tardieux, 1999). However, centrifugation of malaria parasite extracts at 500,000 × *g* resulted in pelleting of most of the actin. Examination of the pellet revealed filaments of ~100 nm in length (Schmitz *et al.*, 2005). This 500,000 × *g* pellet also contained a variety of actin-binding proteins (Schmitz *et al.*, 2005); thus it remains unclear if some of the actin is complexed with these other components. Moreover, it is unclear from this study if the short length of the filaments is an intrinsic property of parasite actin or is due to interaction with other proteins. Purification of malaria actin expressed in yeast also revealed the ability to form small polymers in the presence of labeled phalloidin (Schuler *et al.*, 2005). Neither of these reports provides kinetic data on parasite actins such as the critical concentration, rate of polymerization, or effects of salts and cations on polymerization. Thus, the intrinsic properties of parasite actins remain largely unexplored.

To elucidate the molecular properties of parasite actin, we cloned and expressed TgACT1 in baculovirus and purified it for biochemical and functional studies. We demonstrate that TgACT1 displays unusual kinetic properties that are likely based on parasite-specific structural differences. These differences may explain the atypical dynamics of actin in vivo that govern the unique form of motility utilized by this group of parasites.

MATERIALS AND METHODS

Cell Culture and Materials

SF9 insect cells (BD Biosciences Pharmingen, San Jose, CA) were maintained in TNM-FH media (BD Biosciences Pharmingen) as monolayer cultures. RH strain *T. gondii* parasites were propagated in human fibroblast cell lines and harvested as described previously (Wetzel *et al.*, 2003). Rabbit actin (99% pure) was obtained from Cytoskeleton (Denver, CO). Alexa-conjugated secondary antibodies and labeled phalloidin were obtained from Molecular Probes (Eugene, OR). Chemicals of the highest commercial grade were obtained from Sigma Chemical Co. (St. Louis, MO) unless otherwise stated.

Plasmid Constructions and Transfection

For insect cell transfection, the coding sequence of *TgACT1* was amplified from RH strain *T. gondii* cDNA using primers 5′-CCGCATATGTATGGCGGATGAAGAAGT-3′ (forward) and 5′-GCCGAATTCTTAGAAGCACTTGCGGTG-3′ (reverse) and cloned into the viral transfer vector pAcHLT-C (BD Biosciences Pharmingen). Recombinant viruses were obtained by cotransfection of the pAcHLT-C/TgACT1 with linearized baculogold genomic DNA into SF9 cells following the manufacturer's instructions (BD Biosciences Pharmingen). Expression of His_6-TgACT1 in SF9 cells was confirmed by separation of cell lysates on 10% SDS-PAGE gels and Western blotting with mouse monoclonal antibody (mAb) against pentahistidine (Molecular Probes), followed by peroxidase-conjugated goat anti-mouse IgG (Jackson ImmunoResearch Laboratories, West Grove, PA) and chemiluminescence detection using ECL Plus (Amersham Biosciences, Piscataway, NJ). To visualize expression by fluorescence microscopy, transfected SF9 cells were fixed with 2.5% formaldehyde in phosphate-buffered saline (PBS) for 15 min, rinsed, permeabilized with 0.1% Triton X-100 in PBS for 5 min, and blocked with 5% normal goat serum and 5% fetal bovine serum (FBS) in PBS for 1 h. TgACT1 was labeled with rabbit polyclonal anti-TgACT1 sera (Dobrowolski *et al.*, 1997) followed by secondary labeling with goat anti-rabbit IgG-conjugated to Alexa 488 (Molecular Probes). Cells were mounted in Vectashield (Vector Laboratories, Burlingame, CA) containing DAPI.

His_6-TgACT1 Expression and Purification

SF9 cells were harvested at 3 d postinfection and lysed in G-actin buffer (G-buffer) without DTT (5 mM Tris-Cl, pH 7.5, 0.2 mM $CaCl_2$, 0.2 mM ATP) containing 2% Triton X-100 and protease inhibitor cocktail (E64, 1 μg/ml; AEBSB, 10 μg/ml; TLCK, 10 μg/ml; leupeptin, 1 μg/ml). His_6-TgACT1 was purified using Ni-NTA agarose according the manufacturer's recommendations (Invitrogen, Carlsbad, CA). To remove contaminating proteins, TgACT1 bound to Ni-NTA agarose beads was washed first with native buffer (20 mM $NaPO_4$, 500 mM NaCl, pH 5.5, 0.5% Triton X-100) and then with 0.5 M KCl, and finally with native wash buffer containing 0.2 M imidazole. TgACT1 was eluted with G-buffer containing 1.0 M imidazole and dialyzed overnight in G-buffer at 4°C. Aggregates were removed by centrifugation for 30 min at 4°C at 10,000 × *g* (Eppendorf 5417R Microfuge, Eppendorf, Westbury, NY). The total protein concentration was determined by SYPRO Ruby (Molecular Probes) staining of proteins resolved in SDS-PAGE gels in comparison to known amounts of rabbit muscle actin. For polymerization assays, TgACT1 protein was freshly purified, stored in G-buffer at 4°C, and used within 2–3 d.

To remove the N-terminal His_6 tag, TgACT1 was incubated for 1 h at room temperature with 1 U of thrombin (Sigma, St. Louis, MO) per 10 μg of purified protein. Cleavage with thrombin releases N-terminal extension from the protein including the His_6 tag. After thrombin treatment, the His_6-tag-containing extension and any remaining uncleaved TgACT1 were removed by adding Ni-NTA agarose (50% vol/vol) for 30 min at 4°C followed by centrifugation. The supernatant containing the purified untagged TgACT1 protein, as well as residual thrombin, was used in polymerization assays. A similar concentration of thrombin only was used as a control.

Copolymerization of Rabbit and TgACT1 In Vitro

Rabbit actin or untagged TgACT1 were induced to polymerize alone (2.5 μM) or together (1:1 ratio or rabbit to TgACT1) in 1× F-buffer (100 mM KCl, 2 mM $MgCl_2$, and 2 mM ATP) for 1 h at RT. After polymerization, F-actin was labeled with Alexa 488 phalloidin (Molecular Probes) added at equimolar concentration and incubated overnight at 4°C. After labeling, samples were diluted 1:50 in G-buffer and 10 μl of solution was added to a poly-lysine-coated coverslip. Samples were allowed to adhere for 5 min followed by fixing with 4% formaldehyde and 0.1% glutaraldehyde in PBS for 15 min at RT. Coverslips were blocked with 5% normal goat serum/5% FBS in PBS and incubated with rabbit anti-TgACT1 antibody (Dobrowolski *et al.*, 1997) followed by goat anti-rabbit IgG conjugated to Alexa 594 (Molecular Probes). Samples were mounted in Vectashield (Vector Laboratories), examined with a Zeiss Axioskop (Carl Zeiss, Thornwood, NY) microscope using a 100× Plan-NeoFluar oil immersion lens (1.30 NA). Images were collected with a Zeiss Axiocam using Axiovision v3.1 and processed using Adobe Photoshop v8.0 (San Jose, CA): all samples were processed using linear adjustments in the same manner.

Actin Sedimentation Assay

Actin polymerization was monitored by ultracentrifugation as previously described (Pardee and Spudich, 1982). Purified and desalted His_6-TgACT1 was incubated in G-buffer (5 mM Tris, pH 8.0, 0.2 mM $CaCl_2$, 0.5 mM DTT, 0.2 mM ATP) for 1 h on ice. Aggregates were removed by ultracentrifugation at 100,000 × *g* using a TL100 rotor and a Beckman Optima TL ultracentrifuge (Becton Coulter, Fullerton, CA) for 20 min. Actin polymerization was initiated by adding 1/10th volume of 10× F-buffer to a final concentration of 100 mM KCl, 2 mM $MgCl_2$, and 2 mM ATP (also including the constituents of G-buffer above) and incubation at RT for 1 h. Samples were centrifuged at 100,000 or 500,000 × *g* for 1 h at 25°C. Pellets were solubilized in sample buffer, resolved

on 10% SDS-PAGE gels, stained with SYPRO Ruby according to manufacturer's recommendations (Molecular Probes), and visualized by fluorescence imaging using Image Gauge v4.22 (FLA-5000 phosphorimager, Fuji Film Medical Systems, Stamford, CT). In some experiments, fractions were detected by Western blotting using rabbit anti-TgACT1 antiserum (Dobrowolski *et al.,* 1997) or mAb C4 (Chemicon International, Temecula, CA), followed by peroxidase-conjugated secondary antibodies (Jackson ImmunoResearch Laboratories), and chemiluminescence using ECL Plus (Amersham Biosciences).

Fluorescence Quenching Assay

Actin polymerization was monitored by the decrease in intrinsic florescence as described previously (Frieden *et al.,* 2000). Intrinsic tryptophan fluorescence emission spectra for actins were obtained on a PTI Quantmaster spectrofluorometer (Photon Technology International, Santa Clara, CA): excitation 292 nm (2-nm bandpass), emission scanned from 300 to 400 nm (3-nm bandpass). Samples were resuspended in a 100-μl cuvette (SubmicroQuartz Fluorometer Cell, Starna Cells, Atascadero, CA) and maintained at 25°C. Actin polymerization was initiated by adding 1/10th volume of 10× F-buffer to a final concentration of 100 mM KCl, 2 mM $MgCl_2$, and 2 mM ATP (also including the constituents of G-buffer above) and incubation at room temperature for 15 min. Emission spectra for untagged TgACT1 were adjusted for the inherent fluorescence of a similar concentration of thrombin (a negligible contribution). Samples were adjusted for the emission spectra of matched samples of buffers. The critical concentration was determined by plotting the change in fluorescence upon addition of F-buffer to different concentrations of untagged TgACT1.

Kinetics of Actin Polymerization

Actin was preincubated for 5 min with 1 mM EGTA and 50 μM $MgCl_2$ (to replace bound Ca^{2+} with Mg^{2+}) before inducing polymerization by addition of 2 mM $MgCl_2$. Untagged TgACT1 was polymerized by the addition of $MgCl_2$, to a final concentration of 2 mM, to solutions containing various concentrations of purified actin. Polymerization was monitored by recording fluorescence at 335 nm (292-nm excitation) using a PTI Quantmaster spectrofluorometer (Photon Technology International). The inverse of the change in peak fluorescence (quenching) was plotted versus time.

Electron Microscopy

Negative Staining. Purified recombinant TgACT1 (either tagged or untagged) or rabbit muscle actin were resuspended at 5 μM in G-buffer and polymerized by addition of 1/10th volume of 10× F-buffer for 1 h. For experiments testing the affects of JAS on filament formation, TgACT1 (1.25 μM) was added to JAS (1 μM) and incubated for 1 h to allow polymerization. Filaments were sedimented at 100,000 × *g* and resuspended in 1× F-buffer and placed onto freshly glow-discharged formvar/carbon-coated Cu grids. Samples were allowed to absorb to grids for 5 min (with or without 5 μM phalloidin), washed twice with dH_2O, and stained with 1% aqueous uranyl acetate (UA; Ted Pella, Redding, CA), pH 5.2 for 1 min. Samples were air dried, viewed, and photographed on a JEOL 1200 EX transmission electron microscope (JEOL USA, Peabody, MA). The average length of filaments was determined from scanned negatives using Volocity software version 3.0.2 (Improvision, Lexington, MA).

Freeze-dried Replicas. Freshly egressed parasites were resuspended in mammalian Ringer's solution and allowed to glide on poly-lysine-coated glass for 10 min at 37°C and then disrupted by sonication as described previously (Wetzel *et al.,* 2003). To induce actin filament formation and stabilization in vivo, intact parasites were treated with 1 μM JAS for 5 min and processed as above. Samples were fixed in 2% glutaraldehyde, rapidly frozen in liquid nitrogen, freeze dried, and platinum-coated as described previously (Wetzel *et al.,* 2003). Replicas were examined and photographed with a JEOL CX100 transmission electron microscope (JEOL). The length of filaments was determined from calibrated negatives using Adobe Photoshop v8.0.

Phylogenetic Analysis

Protein sequences for actins representing the vertebrates (β-actin from *Homo sapiens*, gi: 4501885; γ-actin from *Mus musculus*, gi: 54036677), fly (*Drosophila melanogaster*, gi: 156773), worm (*Caenorhabditis elegans*, gi: 6626), plant (*Arabidopsis thaliana*, gi: 30687201), amoeba (*Amoeba proteus*, gi: 33946363), *Dictyostelium* (*Dictyostelium discoideum*, gi: 113218), yeast (*Saccharomyces cerevisiae*, gi: 38372623), ciliates (*Paramecium caudatum*, gi: 15212111; *Tetrahymena thermophila*, gi: 84344), dinoflagellates (*Crypthecodinium cohnii*, gi: 19908693; *Lingulodinium polyedrum*, gi: 37694465) plus selected apicomplexans and related organisms (*Toxoplasma gondii,* gi: 606857; *Plasmodium falciparum* ACT1, gi: 160053; *Cryptosporidium parvum*, gi: 113293; *Cryptosporidium hominis*, gi: 54657132; *Perkinsus marinus*, gi: 38112716). Sequences were retrieved from NCBI or parasite databases in the case of *Eimeria tenella* (http://www.sanger.ac.uk/Projects/E_tenella/) or *Neospora caninum* (http://www.cbil.upenn.edu/apidots/). Sequences were aligned using ClustalX (v1.81; Higgins *et al.,* 1996) using gap opening = 10, gap extension = 0.2, protein matrix Gonnet 250. All regions of the alignment were included in the phylogenetic analysis. Dendrograms were generated in PAUP* 4.0 (Swofford, 1998) by neighbor-joining and parsimony methods and bootstrapped for 1000 replicates. Identical trees were obtained from both analyses.

Molecular Modeling

All sequences of interest were first aligned using ClustalW (Chenna *et al.,* 2003). Based on the sequence alignment, the different levels of conservation were projected on to the ADP actin structure (pdb 1J6Z; Otterbein *et al.,* 2001) for visualization. Similar procedures were used to generate a filament model for TgACT1 based on the Holmes structure (Kabsch *et al.,* 1990). All molecular graphics images were produced using VMD (Humphrey *et al.,* 1996).

RESULTS

Expression, Purification, and Sedimentation of TgACT1

To investigate the properties of *T. gondii* actin outside the confines of the parasite, we expressed the protein in a heterologous insect cell system. TgACT1 containing an N-terminal His_6 tag was cloned under control of the viral polyhedron late promoter and expressed as recombinant protein in SF9 cells. Expression resulted in accumulation of His_6-TgACT1 in the cytosol of SF9 cells as revealed by specific antibody staining (Figure 1A). His_6-TgACT1 was largely soluble in detergent treated cell lysates and was subsequently purified to homogeneity by Ni-resin chromatography as shown by staining with SYPRO Ruby (Figure 1B, lane 3).

In yeast and vertebrate cells, polymerized actin can be functionally separated from globular actin by centrifugation at 100,000 × *g* (Pardee and Spudich, 1982). Recent findings suggest that malaria actin found in lysates of parasite cells forms short filaments that only sediment efficiently at 500,000 × *g* (Schmitz *et al.,* 2005). In order not to inadvertently loose such small filaments, we adopted this approach for monitoring polymerization of TgACT1. Purified TgACT1 was almost entirely soluble in G-buffer and remained in the supernatant after ultracentrifugation at 500,000 × *g* (Figure 1C). In contrast, purified TgACT1 readily pelleted when exposed to high salt conditions (F-buffer) and subjected to ultracentrifugation at 500,000 × *g*, indicating it was polymerized (Figure 1C). Purified TgACT1 also polymerized in response to addition of 2 mM Mg^{2+} or 100 mM KCl to G-buffer, resulting in sedimentation by ultracentrifugation (Figure 1C). Similarly, when TgACT1 was incubated in F-buffer and centrifuged at 100,000 × *g*, it was efficiently pelleted (unpublished data).

An inherent property of actin is the ability to spontaneously assemble into filaments above a critical concentration (Cc), which varies from 0.1 to 0.6 μM at the barbed (+ end) and pointed (− end) end of the molecule, respectively (average Cc is ~0.12 μM; Pollard *et al.,* 2000). We tested the polymerization of purified TgACT1 over a range of protein concentrations in F-buffer. Plotting the extent of polymerization based on the fraction of actin that sedimented after ultracentrifugation at 500,000 × *g* versus to the total actin concentration revealed that TgACT1 polymerized in a linear manner above a concentration of 0.03 μM (Figure 1D). When different concentrations of TgACT1 were polymerized by addition of F-buffer and centrifugation at 100,000 × *g*, the Cc was ~0.4 μM (unpublished data).

Polymerization Kinetics of TgACT1

Previous studies have shown that addition of a N-terminal His tag to yeast actin does not affect its polymerization or function in yeast (Buzan and Frieden, 1996; Buzan *et al.,* 1999). Nevertheless, we tested whether the presence of the N-terminal tag affected polymerization of TgACT1 by mon-

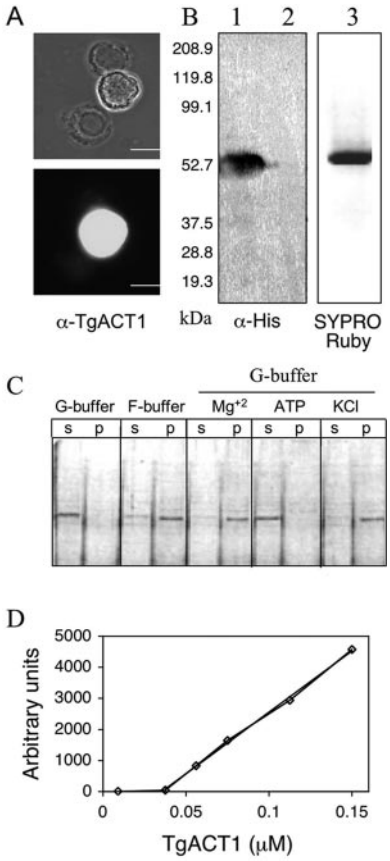

Figure 1. Expression, purification, and in vitro polymerization of His_6-TgACT1. (A) Phase-contrast and immunofluorescence images of His_6-TgACT1 expression in SF9 cells. Stained with rabbit α-TgACT1 followed by secondary antibody conjugated to Alexa 488. Scale, 20 μm. (B) TgACT1 expressing SF9 (lane 1) and control SF9 (lane 2) cell lysates resolved by 10% SDS-PAGE and Western-blotted with anti-His tag antibody (α-His). Ni-resin chromatography purified TgACT1 (lane 3) resolved on 10% SDS-PAGE and stained with SYPRO Ruby. (C) Separation of polymerized and soluble His_6-TgACT1 (0.5 μM) after addition of salts to G-buffer. After ultracentrifugation, the supernatants (s) and pellets (p) were analyzed on 10% SDS-PAGE and stained by SYPRO Ruby. (D) Different concentrations of His_6-TgACT1 were polymerized in F-buffer, and the ultracentrifuged samples were analyzed by SDS-PAGE followed by Western blotting with anti-actin mAb C4 and peroxidase-conjugated goat anti-mouse IgG. The pellet fractions were quantified by phosphorimager analysis and plotted as relative light units (*Y*-axis). Actin polymerization occurred linearly above 0.03 μM (*X*-intercept). Curve fit using linear regression analysis.

itoring the quenching of tryptophan fluorescence, which is an inherent property of actins. TgACT1 contains four tryptophan residues like other actins, and during polymerization their intrinsic fluorescence undergoes quenching (Doyle *et al.,* 2001). The N-terminal His_6 tag extension was cleaved with thrombin to generate an untagged form of TgACT1. Quenching of tryptophan was monitored by decreased fluorescence after addition of F-buffer salts to stimulate actin polymerization. Although tagged TgACT1 exhibited lower intrinsic fluorescence when compared with untagged protein, both forms underwent quenching after the addition of F-buffer to induce polymerization (unpublished data).

Because the sedimentation assay shown in Figure 1 could be influenced by aggregation, we also determined the Cc by plotting the quenching of intrinsic tryptophan fluorescence of different concentrations of TgACT1 after addition of F-buffer (Figure 2A). Plotting the change in fluorescence versus concentration of TgACT1 provided an independent estimate of the Cc of ~0.04 μM for untagged TgACT1 (Figure 2B). Similar experiments using His_6-TgACT1 revealed the average Cc to be ~0.03 μM (unpublished data). These results confirm that the tag has little effect on polymerization in vitro. We also monitored the Cc of untagged TgACT1 in the presence of 10 μM cytochalasin D (Figure 2C), which decreases polymerization at the barbed but still allows assembly at the pointed end. The Cc at of TgACT1 in the presence of CytD was ~0.18 μM, which provides an estimate of the Cc at the pointed end (Figure 2C).

The rate of TgACT1 polymerization in the presence of 1.0 μM ATP was dependent on protein concentration and at low protein concentrations exhibited a noticeable lag (Figure 2D). This lag phase corresponds to the slow nucleation step, after which polymerization occurs at a more rapid rate during the elongation phase (Cooper *et al.,* 1983; Tobacman and Korn, 1983). Previous studies have shown that the size of the critical nucleus for initiating elongation can be estimated from the slope of a log-log plot of the maximum polymerization rate versus actin concentration (Nishida and Sakai, 1983). We plotted the Log [Vmax] versus Log [actin] from data as in Figure 2D, determined the slope of this plot and estimated that the nucleus size is ~3 (nucleus = (slope − 1) × 2; Nishida and Sakai, 1983), similar to that exhibited by conventional actins.

Bacterial actin-like proteins such as ParM are highly sensitive to ATP and show dynamic instability due to high turnover of nucleotide (Garner *et al.,* 2004). This feature leads to rapid polymerization that often overshoots the plateau followed by rapid disassembly (Garner *et al.,* 2004). To determine the sensitivity of TgACT1 to nucleotide, we monitored polymerization over time in 1.0 mM ATP versus ADP. Polymerization of TgACT1 was more rapid and reached higher plateau in ATP versus ADP (Figure 2E). Once polymerized, TgACT1 remained stable in the presence of ATP (Figure 2E). Tryptophan quenching was also used to measure the Cc of actin polymerization in the presence of ADP, conditions where the rate of polymerization at both ends is equal (Pollard, 1984). As shown in Figure 2F, the Cc in the presence of ADP shifted by about fourfold to a value of 0.16 μM. This shift is similar to that observed for vertebrate actins (2–10-fold) but less than for *Acanthamoeba* (almost 50-fold; Pollard, 1984).

Collectively, these studies reveal that the major difference from conventional actins exhibited by TgACT1 is a very low Cc, making it permissive to form new filaments at low concentration.

TgACT1 Forms Short Unstable Filaments In Vitro

Staining with fluorescent phalloidins, which bind selectively to F-actin, is typically used to reveal polymerized actin. Rabbit or untagged TgACT1 were polymerized by addition of F-buffer, stained with fluorescent phalloidin, and examined by epifluorescence microscopy to reveal filaments. Rabbit actin readily polymerized into large mats of interwoven filaments that were strongly stained with labeled phalloidin (Figure 3A), TgACT1 remained in small punctate dots of fluorescence that were recognized with rabbit anti-TgACT1 (Figure 3B). The small foci formed by TgACT1 were only weakly stained with phalloidin (Figure 3B), consistent with a previous report indicating that malaria actin binds phalloidin less strongly than yeast actin

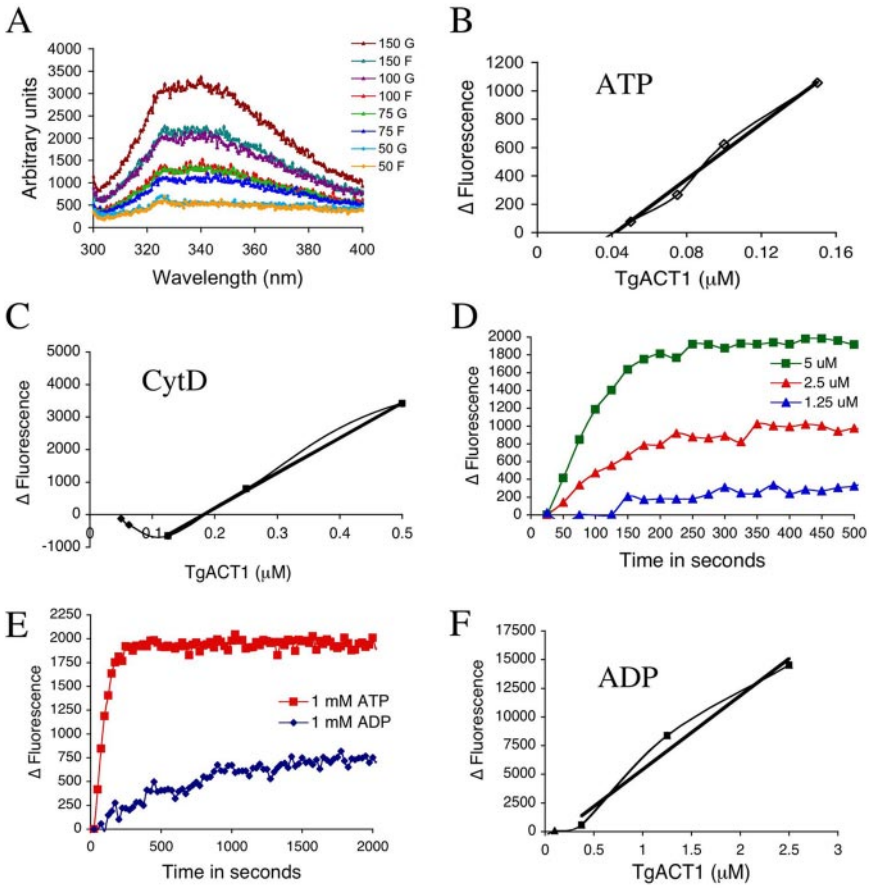

Figure 2. Polymerization properties of TgACT1. (A) Tryptophan quenching curves are shown for various concentrations (in nM) of untagged TgACT1 in G- or F-buffer. Readings were conducted 15 min after addition of F-buffer salts. *Y*-axis values are arbitrary fluorescence units. (B) Plotting the change in peak fluorescence between G-buffer and F-buffer (shown in A) versus concentration of untagged TgACT1, reveals the critical concentration to be ~0.04 μM (*X*-intercept). (C) Plot of the change in tryptophan quenching versus concentration of TgACT1 in the presence of 10 μM CytD. The resulting Cc was ~0.18 μM (*X*-intercept). (D) Polymerization of different concentrations of TgACT1 in 1.0 mM ATP and 2 mM $MgCl_2$ over time as determined by tryptophan quenching. At low concentrations, a noticeable lag is observed. (E) Dependence of polymerization on ATP versus ADP. Curves show tryptophan quenching over time for 5.0 μM TgACT1. (F) Determination of the TgACT1 Cc in the presence of 1.0 mM ADP as determined by tryptophan quenching. The resulting Cc was ~0.16 μM (*X*-intercept). The plots in B–F show the absolute value of the change in intrinsic fluorescence on the *Y*-axis in arbitrary fluorescence units.

(Schuler *et al.*, 2005). TgACT1 failed to copolymerize with filaments formed by rabbit actin (Figure 3C). Our results indicate that TgACT1 does not readily copolymerize with vertebrate actin and only forms small foci under conditions that normally result in formation of long filaments by conventional actins.

The ability of purified TgACT1 to polymerize after addition of F-buffer and sedimentation at 100,000g was further analyzed by negative staining and examination by transmission EM. While in some cases only globular aggregates were found (unpublished data), in other instances, actin-like filaments were clearly observed (Figure 4A). TgACT1 filaments were relatively short (~0.1 μm; Figure 4B, Table 1) and often appeared kinked or as broken fragments (Figure 4A). When TgACT1 was polymerized in F-buffer, sedimented at 100,000 × *g*, and resuspended in F-buffer containing phalloidin during preparation, filaments appeared more linear and had distinct edges (Figure 4A). Phalloidin-stabilized TgACT1 filaments were slightly longer with an average size of 0.2 μm (Figure 4B, Table 1). Filaments formed by TgACT1 were unbranched with an approximate width of 9 nm and repeated cross-striations, characteristic of conventional actin (Figure 4, A and B). Filaments formed by highly purified rabbit skeletal muscle actin were also unbranched but were on average 10-fold longer than TgACT1 filaments (Figure 4, A and B; Table 1).

JAS has been reported to induce actin filament formation in the parasite, resulting in hyperkinetic but dysfunctional behavior by the parasite (Wetzel *et al.*, 2003). We tested the affects of JAS on actin filament formation in vitro by mixing it with purified TgACT1 and inducing polymerization by addition of F-buffer. JAS-induced filaments were more abundant when examined by negative staining and EM (Figure 4A). Additionally, JAS-treated filaments were approximately twice the width of normal filaments. On higher magnification it was evident this was due to bundling or cross-linking of two filaments together (Figure 4A, bottom panel). In other examples, multiple filaments were observed together in tangles (unpublished data). The average length of JAS-treated actin filaments was substantially longer than control (0.24 vs. 0.1 μm; Table 1). This increase was largely due to a broader distribution in sizes that also included filaments of ~0.5–0.6 μm in length (Figure 4).

Actin Forms Short Filaments in the Parasite

We have previously shown that when parasites are allowed to glide on substrates in vitro and then rapidly removed by gentle sonication, they leave behind small membrane footprints that are decorated with short actin-like filaments (Wetzel *et al.*, 2003). These filaments have the hallmark features of actin, including cross-striations, 9-nm diameter, and sensitivity to CytD (Wetzel *et al.*, 2003). Examination of such membrane footprints revealed clusters of actin filaments (Figure 5A), and enlarged views of these filament arrays indicated they were typically parallel and unbranched (Figure 5B). The length of actin filaments formed by gliding parasites was approximately ~0.185 μm (Figure 5E, Table 1), which is similar to filaments formed by TgACT1 in vitro.

We also examined the formation of actin filaments in parasites treated with JAS and then processed to reveal filaments beneath the plasma membrane. JAS-induced fila-

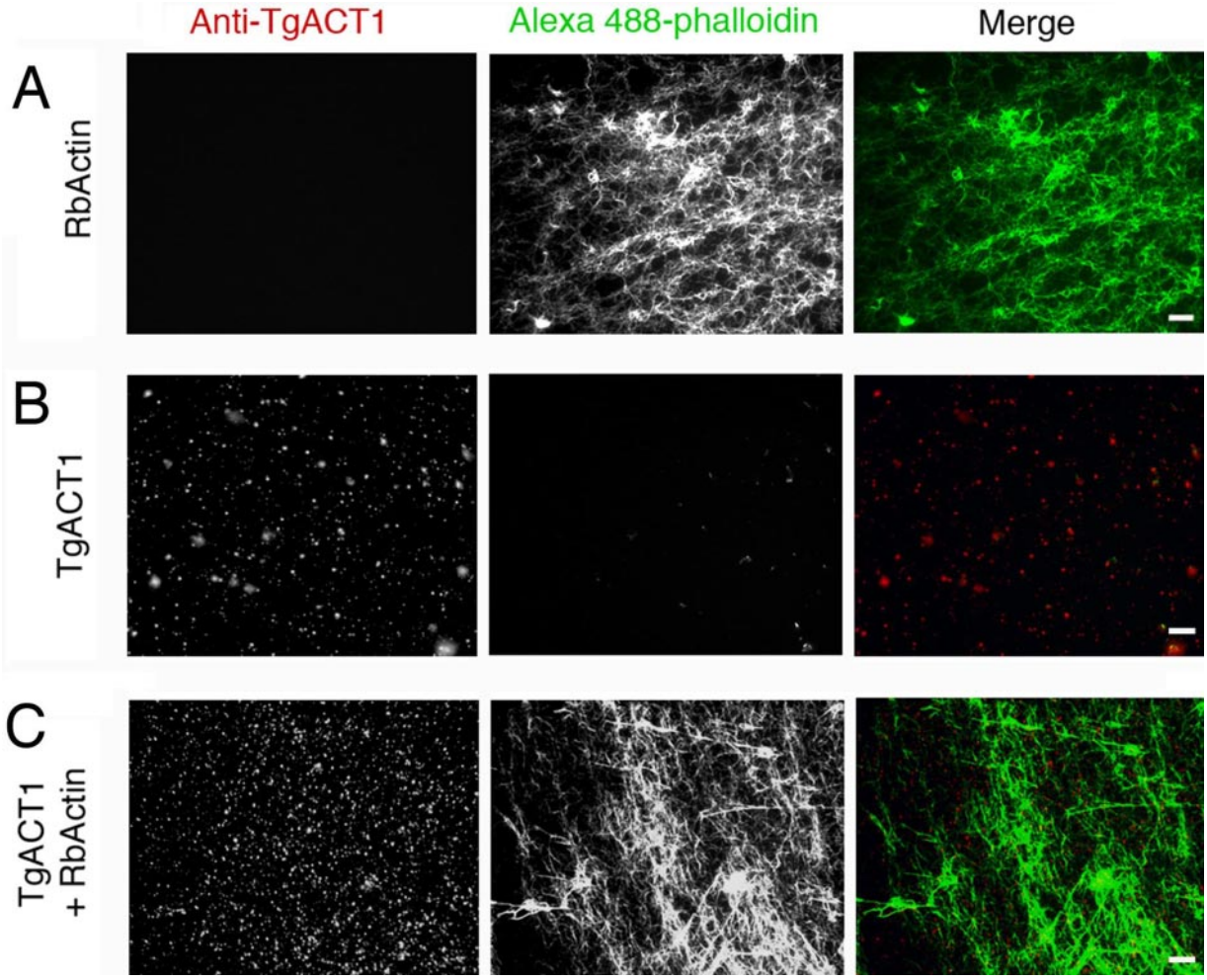

Figure 3. In vitro polymerization of actin detected by epifluorescence microscopy. (A) Polymerization of rabbit actin (RbActin) alone leads to a large network of intertwined filaments revealed by staining with Alexa 488-phalloidin. (B) In contrast, polymerization of TgACT1 leads to formation of small foci that stain weakly with phalloidin but that react to rabbit anti-TgACT1 antibodies (revealed by staining with Alexa 594-conjugated goat anti-rabbit IgG). (C) Polymerization of a 1:1 mixture of these two proteins together did not result in copolymerization. Scale bars, 5 μm.

ments were both more abundant and highly disorganized in their appearance (Figure 5C). JAS-induced filaments were scattered in large clumps or tangled piles (Figure 5C). JAS-induced filaments were almost twice the normal diameter and resembled two tightly interacting filaments (Figure 5C). Higher magnification of these JAS-treated filaments revealed they have the characteristic striations and helical twist (Figure 5D). JAS treatment of parasites resulted in a slight increase in filament length compared with control cells (Figure 5E, Table 1).

Molecular Phylogeny of Apicomplexan Actins

The unusual polymerization properties of TgACT1 suggested that differences in the molecular structure might be responsible for its unique behavior. To identify residues in the primary sequence might play a role in its unusual polymerization properties, we analyzed parasite actins phylogenetically to define residues that were specific to the phylum Apicomplexa. Included in this analysis were several apicomplexan parasites (*Neospora, Cryptosporidium, Plasmodium*, and *Eimeria*) as well as ciliates (*Tetrahymena, Paramecium*) and dinoflagellates (*Lingulodinium, Crypthecodinium*), which are closely related to the Apicomplexa (Baldauf *et al.,* 2000). We included only conventional actins here as there are numerous other actin-like proteins in the genomes of apicomplexans (J. L. Gordon, L. D. Sibley, unpublished results). We also included conventional actins from plant, fly, worm, yeast, amoeba, and vertebrates. Clustal alignment and phylogenetic comparisons verified that apicomplexan actins form a group that is most similar to ciliates and dinoflagellates (Figure 6A and Supplementary Figure 1).

Computational Modeling of Parasite Actin

Using the multiple sequence alignment of actins, we projected conserved residues on to the crystal structure of ADP muscle actin (Otterbein *et al.,* 2001). Residues that were distinct from conventional actins and conserved among apicomplexans were colored red/orange (red, most apicomplexans; orange, all apicomplexans), whereas those conserved among ciliates, dinoflagellates, and apicomplexans were colored yellow (Figure 6B). The majority of these substitutions occurred on the surface of the exposed domains of the actin monomer, including the DNAse I binding loop in subdo-

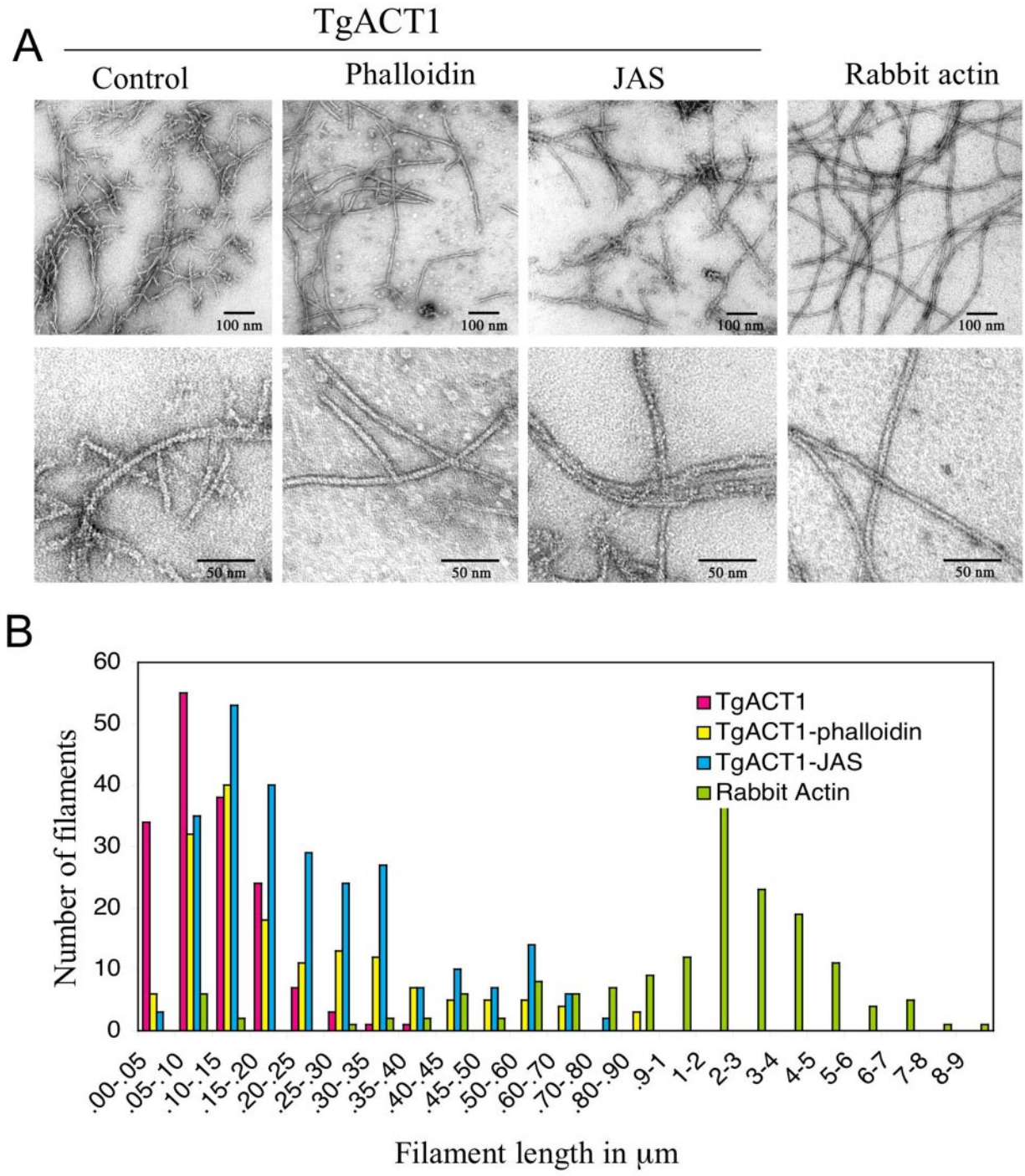

Figure 4. Ultrastructural examination of polymerized TgACT1 filaments compared with rabbit actin. (A) Filaments formed by TgACT1 were short, unbranched, and often appeared bent or broken (TgACT1 control). When polymerized TgACT1 filaments were mixed with 5 μM phalloidin on the grid, they were straight and had more distinct edges, indicating they were stabilized. TgACT1 filaments were observed to form pairs or small bundles when polymerized in the presence of JAS (1 μM; see bottom panel for enlargement). Rabbit actin formed long straight filaments with a characteristic helical spiral. Enlarged views (bottom panels) demonstrate the repeat striations, helical pattern, and ~9-nm diameter of the filaments formed by TgACT1 and rabbit actin. After polymerization of 5 μM actins in F-buffer, 100,000 $\times$ *g* pellets were resuspended in 1$\times$ F-buffer, negatively stained with uranyl acetate, and examined by EM. (B) Histogram showing the distribution of filament lengths between control, phalloidin (5 μM) or JAS (1 μM) treated TgACT1 and rabbit muscle actin. TgACT1 filaments were more than 10-fold shorter than rabbit actin filaments formed under similar conditions. Treatment of TgACT1 with phalloidin or JAS increased the average size.

main 2 and several portions of subdomains 1, 3, and 4, as well as the hydrophobic plug that lies in the cleft between subdomains 3 and 4 (Figure 6B). One notable feature of apicomplexan actins (with the exception of *Cryptosporidium*) is the substitution of an N residue for M at position 17, which protrudes into the nucleotide-binding pocket.

Table 1. Average length of actin filaments

Preparation	Average length (μm)	Range (μm)	n
TgACT1 in vitro	0.105 ± 0.064	0.020–0.363	164
TgACT1 in vitro + phalloidin	0.144 ± 0.102	0.030–0.705	157
TgACT1 in vitro + JAS	0.241 ± 0.153	0.045–0.785	257
Rabbit actin in vitro	2.020 ± 1.710	0.050–8.920	164
TgACT1 in vivo	0.181 ± 0.082	0.072–0.420	76
TgACT1 in vivo + JAS	0.199 ± 0.830	0.600–0.464	62

Average lengths of actin filaments in the preparations listed were determined by measurement from negatively stained EM negatives. All values for TgACT1 were performed on untagged protein.

Modeling Filament Interactions

To model how differences in the TgACT1 sequence might influence filament assembly, we constructed a TgACT1 filament using the Holmes filament model as a template (Kabsch *et al.*, 1990; Figure 7A). Many of the residues conserved among apicomplexans fall on the outside surface of the filament and thus are likely to have effects on the interaction with actin-binding proteins. However, there are two key substitutions that we predict would affect both the filament structure and stability. In muscle actin, there is strong ionic and hydrogen bonding between residues R39 in subdomain 2 and E276 in subdomain 3 (muscle numbering) between adjacent monomers: this interaction is thought to stabilize lateral interactions within the filament (Figure 7B). In yeast actin, E276 corresponds to Q276, conserving the hydrogen bonding with R39, but at the loss of the additional electrostatic interaction. In stark

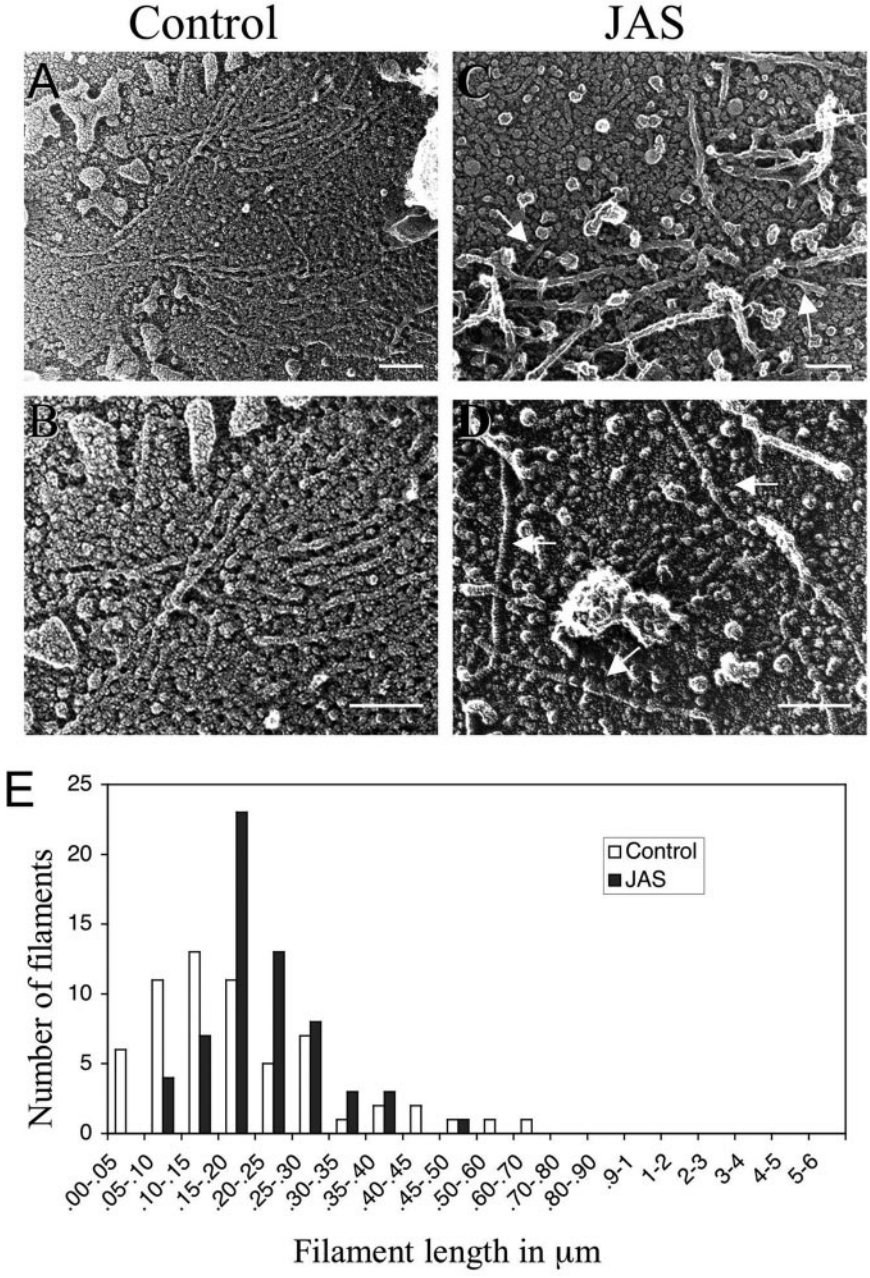

Figure 5. Visualization of actin filaments formed in parasites. Actin filaments were observed on the inner surface of the parasite plasma membrane that remained attached to the substrate after removal of the parasite by gentle sonication. Images were generated by rapid freeze-drying and platinum-coated replicas that were examined by EM. Scale bar, 100 nm in all panels. (A) In control cells, short filament arrays were detected on the inner surface of the parasite plasma membrane. (B) Enlargement of image shown in A showing the parallel arrangement of filaments. (C) Treatment with JAS (1 μM) resulted in a tangled web of short filaments. Most filaments were twice the normal diameter indicating they were bundled. Arrows denote single filaments. (D) Enlargement of a preparation similar to C showing individual TgACT1 filaments formed in the presence of JAS (arrows). (E) Average lengths of TgACT1 filaments formed in control (□) versus JAS-treated (■) parasites, JAS treatment resulted in a slight increase in average length.

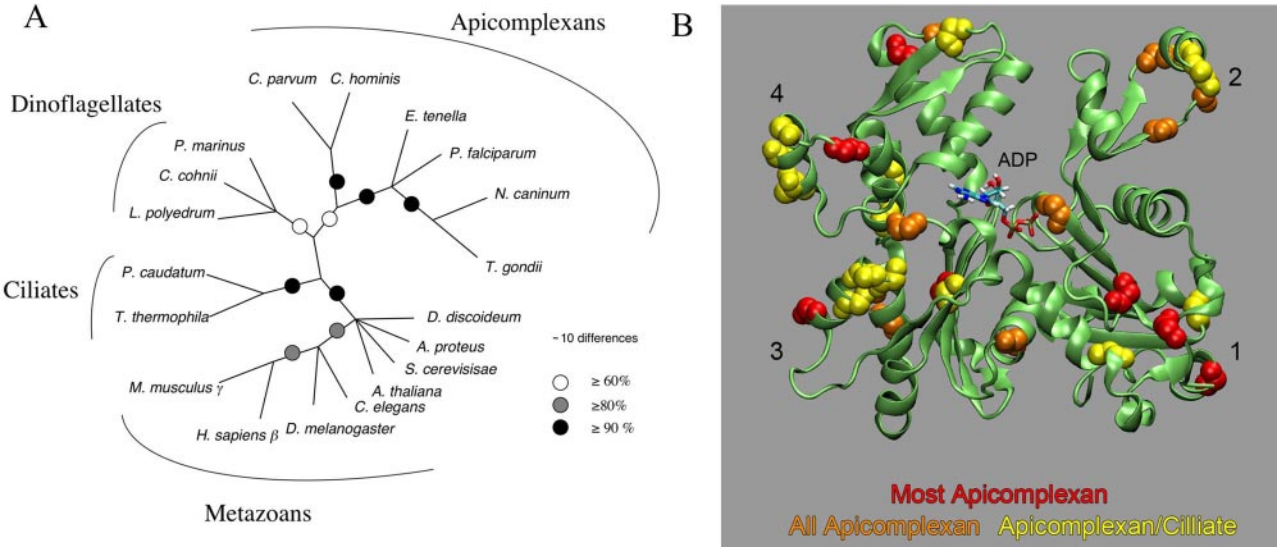

Figure 6. Phylogenetic and modeling analyses reveal conserved residues in parasite actins. (A) Phylogenetic analysis depicts the similarity of parasite actins to ciliates and dinoflagellates. The shaded circles show confidence estimates for trees (N = 1000 permutations). Sequence accession numbers for each actin are given in *Materials and Methods.* (B) Model of TgACT1 structure depicting apicomplexan specific residues. Amino acids conserved among various organisms are projected on to an ADP actin structure based on their sequence alignment. Color code refers to conservation of residues as follow: red, conserved in most apicomplexans (typically all except *Cryptosporidium*); orange, conserved in all apicomplexans; yellow, conserved in apicomplexans, ciliates, and/or dinoflagellates.

contrast to both yeast and muscle actin, R40 is conserved in *T. gondii*, whereas E276 corresponds to R277, leading to a highly unfavorable electrostatic interaction (Figure 7C). We have allowed for some side chain reorganization in our *T. gondii* actin model, but the close proximity of these basic groups should significantly destabilize the lateral interactions within the filament.

In addition to these changes, a portion of the hydrophobic loop is not conserved in apicomplexan actins. According to the Holmes model, this region (262–272 in muscle actin) is predicted to bind in the pocket formed by adjacent monomers and stabilize the two strands of the filament. The sequence at the tip of this hydrophobic loop is FIGM (266–269) in muscle actin while in TgACT1 the corresponding residues are FLGK (267–270; Figure 7D). The K at position 270 is expected to disrupt the hydrophobic interactions made by the rest of the loop, further destabilizing the interactions between the two strands of the actin filament.

DISCUSSION

To elucidate the kinetic properties of parasite actins, we expressed TgACT1 in insect cells and purified it to homogeneity. Recombinant TgACT1 polymerized in vitro in response to the addition of salt and cations. TgACT1 polymerized at a 3–4-fold lower concentration than conventional actins, yet filaments formed by TgACT1 were short and unstable. Molecular modeling suggests that the unusual properties of TgACT1 may be mediated by key structural differences that affect interactions within the filament. These properties define a novel form of filamentous actin that is adapted for rapid cycles of assembly and disassembly and that regulates the novel form of gliding locomotion utilized by apicomplexan parasites.

Conventional actin polymerization requires physiological salt concentrations and is enhanced by Mg^{2+} (Pollard *et al.*, 2000). TgACT1 responded normally to addition of KCl or Mg^{2+} and underwent polymerization as determined by sedimentation, tryptophan quenching, and formation of filaments observed by EM. Estimation of the nucleation size indicates that TgACT1 has a conventional trimeric nucleus. After a brief lag phase, it assembles in a linear manner as a double-stranded helical filament. TgACT1 polymerized above a concentration of 0.03 μM, which is 3–4-fold lower than the Cc observed with vertebrate or yeast actins (Pollard *et al.*, 2000). The Cc of TgACT1 was increased in the presence of ADP (~0.16 μM) and by incubation in CytD (~0.18 μM), consistent with the rate of polymerization being slower at the pointed end. Collectively these findings indicate that the main kinetic difference in TgACT1 is a 3–4 lower Cc that drives assembly of filaments at lower concentrations than conventional actins.

Bacterial actin homologues are structurally related to eukaryotic actins but show many unusual kinetic properties. For example, MreB, which forms spiral filaments involved in maintaining bacterial cell shape, has a very rapid assembly with essentially no nucleation phase (Esue *et al.*, 2005). MreB has a Cc of 3 nM and displays relatively normal ATPase rates (Esue *et al.*, 2005). ParM, a bacterial actinlike protein involved in DNA segregation, also has a very rapid polymerization rate, some 300 times that of vertebrate actin, yet it displays dynamic instability driven by ATP hydrolysis (Garner *et al.*, 2004). Bacterial actin homologues are not phylogenetically similar to parasite actins, thus it is not surprising that TgACT1 does not display these extreme behaviors. Instead, although TgACT1 polymerized more readily in ATP than ADP, it was stable after assembly and does not appear to undergo dynamic instability like ParM. However, the kinetic and structural properties of TgACT1 are well suited for its role in gliding motility.

Despite previous reports indicating that malaria actin only sediments efficiently at 500,000 × *g* (Schmitz *et al.*, 2005), our EM and sedimentation experiments revealed that TgACT1

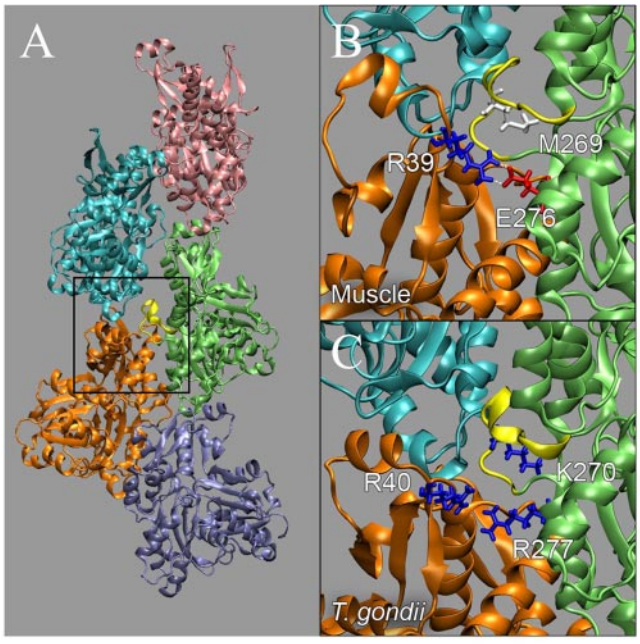

D Hydrophobic loop 267-270

Muscle	F	I	G	M	(H)
Yeast	V	L	G	L	(Y)
TgACT1	F	L	G	K	(T)

Figure 7. Conserved features of apicomplexan actins that are predicted to destabilize filaments. (A) Actin filament models were based on the Holmes structure. Molecular modeling was used to determine contact points between adjacent monomers. The hydrophobic plug is shown in yellow. (B) Salt bridge between R39 and E276 of adjacent monomers in the filament formed by muscle actin. Within the hydrophobic plug (yellow) the position 269 is M. (C) In TgACT1, the alteration of residue 277 in subdomain 3 from E to R eliminates the potential salt bridge with R40 in subdomain 2, resulting instead in charge repulsion between adjacent monomers in the filament. Within the hydrophobic plug (yellow), residue 270 is changed from M to K: the resulting positive charge is likely to alter interaction with the hydrophobic pocket in the adjacent monomer. Both of these changes have the potential to destabilize the filament. (D) Residues of the hydrophobic plug for muscle, yeast, and TgACT1 showing the hydrophobic nature of this region that is disrupted by alteration of M/L to K in *T. gondii*.

filaments of ~50–100 nm in length were pelleted at 100,000 × *g*. This difference may reflect the fact that our studies were performed using highly purified protein that was polymerized in vitro, rather than in cell lysates where a variety of other proteins might influence the dynamics of actin. When compared with conventional rabbit actin filaments, TgACT1 filaments were much shorter and also tended to be unstable, often breaking into short fragments or forming aggregates. In this regard, TgACT1 filaments resemble the early stages of filament formation by vertebrate actin, which are initially in an open conformation that appears ragged but are gradually stabilized by annealing through lateral interactions between monomers within the filament (Schoenenberger *et al.*, 2002). The inherent instability of TgACT1 filaments may result from failure to generate cross-filament interactions that provide for proper annealing. One of the interactions that has been suggested to stabilize cross-filament interactions is mediated by the hydrophobic loop, a region between subdomains 3 and 4 (Orlova *et al.*, 2004). Thus, it may be significant that TgACT1 has a nonconservative substitution introducing a charged K residue at 270 (M269 in vertebrate actin) near the end of hydrophobic loop (discussed further below). When artificially stabilized by treatment with JAS, TgACT1 formed filaments that were well defined with typical striations and a slight helical twist. JAS treatment induced polymerization of stable actin filaments in vitro, leading to an increase in the overall length of filaments and to cross-linking between filaments. However, JAS-treated TgACT1 filaments were still shorter than rabbit actin, indicating they are only partially stabilized by this treatment. Moreover, only a slight increase in the length of JAS-treated TgACT1 filaments was noted in vivo; this might reflect the activity of actin-binding proteins that enhance turnover or cap growing filaments.

The reliance of apicomplexan parasites on actin polymerization for motility, combined with the unusual dynamics of actin turnover, results in extreme sensitivity to JAS-induced actin stabilization. JAS inhibits parasite gliding within minutes with an IC_{50} of 50 nM (Wetzel *et al.*, 2003). Vertebrate cells are not affected by such low concentrations of JAS until after many hours of incubation, and even then the phenotype is modest (Bubb *et al.*, 2000). The binding site for JAS has not been precisely mapped, although it is thought to overlap with that of phalloidin based on competition studies (Bubb *et al.*, 1994). Although *T. gondii* (present report) and *P. falciparum* (Schuler *et al.*, 2005) are less sensitive to phalloidin than vertebrate cells, they are much more sensitive to the effects of JAS. Further studies may reveal whether the conserved molecular substitutions of apicomplexan actins are responsible for these differences in sensitivity to actin-stabilizing drugs. Moreover, this sensitivity may be exploitable to selectively disrupt parasite actin regulation and thus prevent infection.

Phylogenetic analysis of actins reveals that despite a high level of identity to conventional actins, key differences are conserved between apicomplexans and their close relatives ciliates and dinoflagellates. Although extensive studies have been performed on yeast, acanthamoeba, and vertebrate actins (Pollard *et al.*, 2000), very little is known about actins in early branching protozoa. Previous studies on *Tetrahymena* actin have revealed that it fails to bind DNAse I or phalloidin (Hirono *et al.*, 1989), in contrast to conventional actins, suggesting these differences are due to ciliate-specific residues. TgACT1 binds to DNAse I agarose sufficiently well to allow purification (N. Sahoo, unpublished results), although *Plasmodium* actin was shown to bind DNAse I less avidly than yeast actin, likely due to differences in subdomain 2 (Schuler *et al.*, 2005). *Tetrahymena* actin is able to copolymerize with vertebrate actins (Hirono *et al.*, 1990). However, TgACT1 failed to copolymerize to any significant extent with rabbit actin in vitro, suggesting that apicomplexan-specific residues disrupt heterologous interactions.

Apicomplexan actins share a number of differences that occur at the monomer surface where they might affect protein-protein interactions either within the filament or with actin-binding proteins. It has been suggested that substitution within the DNAse I loop of residue H40 to N in apicomplexan actins might affect filament formation by altering interactions with subdomain 3 in the adjacent monomer (Schmitz *et al.*, 2005). Additionally, alteration of Q41 to P may affect filament formation because cross-linking studies

have implicated this residue in forming monomer-monomer contacts within the filament (Schmitz *et al.,* 2005).

By examining residues that are conserved in apicomplexans relative to close relatives such as ciliates, we identified several additional residues of potential importance for actin filament formation. Modeling TgACT1 filaments based on the Holmes model identified six unique and conserved residues in apicomplexan actins that are at monomer contact points within the filament: H195, G200, N247, K270, A272, and R277. Three of these substitutions are predicted to have major effects on the filament structure. R277 in *T. gondii* corresponds to E276 in muscle actin where this residue makes a very favorable intermonomer salt bridge and hydrogen bonding interaction with R39. In TgACT1 this salt bridge is replaced with an unfavorable R-R pairing that should tend to weaken the interaction between adjacent monomers across the two strands of the filament. Molecular modeling did not allow for more than minor side chain reorganization within the *T. gondii* actin model; however, because these basic groups are so close together (~3–4 Å in the muscle model), it is likely that they would significantly destabilize the binding between the two strands of the actin filament or alternatively change the conformation of the filament. Additional structural, mutational, and computational studies will be necessary to test these predictions.

A second alteration in apicomplexan actins is the lack of conservation at the tip of the hydrophobic plug where the normal M at position 269 in muscle (L in yeast) actin becomes K in *T. gondii*. According to the Holmes model, this alteration in the hydrophobic plug should lead to additional destabilization between subunits across the filament. Previous studies in yeast have shown that mutations of residues within the hydrophobic plug have variable phenotypes that partially support the Holmes model, yet also reveal differences in relative importance of specific residues. For example, alteration of L267 to G in yeast actin results in a cold-sensitive phenotype characterized by unstable filaments (Chen *et al.,* 1993). Other mutations within this hydrophobic stretch including L269D or L269K had little discernable effect on actin polymerization in vitro (Kuang and Rubenstein, 1997). Although this result might suggest that residues at the C-terminal end of the hydrophobic plug play a less important role, the specific alteration seen in TgACT1 (L/M to K) has not been tested in the context of other alterations seen in parasite actins. Thus, it is conceivable that alteration of this hydrophobic residue from L270K may have a profound affect when combined with other changes seen in parasite actins as described above. Importantly, the instability of TgACT1 filaments was partially restored in the presence of phalloidin and JAS, which would be expected to stabilize cross-subunit interactions within the filament, based on previous results with yeast (Kuang and Rubenstein, 1997).

Our studies of highly purified TgACT1 indicate that formation of short filaments is an inherent property of parasite actin. The filaments formed by TgACT1 in vitro share features with short filaments that are detected beneath the membrane during motility of *T. gondii*, including a similar length distribution and unbranched structure (Figures 4 and 5 and Table 1; Wetzel *et al.,* 2003). Although a number of factors could influence the formation of filaments in vivo, all of the available evidence suggests that parasites rely on short filaments to power cell motility and invasion. TgACT1 is uniquely suited for rapid assembly because of its relatively low critical concentration, which is 3–4-fold lower than that in conventional actins. However, the filaments formed by TgACT1 are inherently fragile and remain short and unbranched. Filament instability is likely due to alterations in residues that mediate binding between adjacent monomers and that normally stabilize the filament. These alterations are largely conserved in apicomplexans, providing an explanation for the absence of stable, long filaments in these parasites. Previous studies demonstrate that the formation of new actin filaments regulates gliding motility (Wetzel *et al.,* 2003), which relies on a small myosin that is anchored in the inner membrane (Meissner *et al.,* 2002; Gaskins *et al.,* 2004). TgMyoA is a nonprocessive motor, implying that it needs a high local concentration of filaments to power motility (Herm-Gotz *et al.,* 2002). Thus, the short filaments formed by TgACT1 are ideally suited to support gliding motility.

Although TgACT1 is highly permissive for formation of new filaments, the absence of stable filaments in the parasite is likely due to both a combination of the instability of filaments and regulation by actin-binding proteins. The cytoplasmic concentration of actin in the parasite is ~8–10 μM (N. Sahoo, unpublished result), a value far above the Cc. This result strongly implies that like in other cells, G-actin is sequestered by actin-binding proteins. The recent completion of the *T. gondii* genome has revealed a remarkably simple set of actin-binding proteins (http://ToxoDB.org) including actin-depolymerizing factor (Allen *et al.,* 1997), capping protein (β subunit (AAU93916.1), α subunit (AAU93918)), profilin (AY937257), coronin (AAU93915.1), and several actin-like proteins (ALP1 [AAW23163] and unpublished data). Future studies will be important to establish the role of these proteins in regulating the dynamics of actin in vivo, where the initiation and turnover of actin filaments are tightly regulated to control motility.

The kinetic properties of TgACT1 are consistent with the need to rapidly generate new filaments to initiate gliding and to subsequently destroy these filaments to prevent unwanted motility. Rapid turnover of filaments is evidently crucial as treatments that stabilize actin filaments (JAS) greatly disrupt the normal coordinated behaviors of gliding (Wetzel *et al.,* 2003). Thus, it is likely that the dynamic instability of TgACT1 filaments is responsible for the rapid turnover of filaments in vivo and is a key adaptation of gliding motility in these cells. Understanding the fundamental structural and kinetic differences in parasite actins may thus allow selective targeting of this molecule to prevent motility and hence block infection by this important group of pathogens.

ACKNOWLEDGMENTS

We are grateful to John Cooper who provided reagents, expert advice on methodology, and critical review of the manuscript. We also thank Carl Frieden, Peter Rubenstein, and Emil Reisler for helpful comments; Nandini Bhattacharya, Jenny Gordon, and Kyoungtae Kim for technical advice and helpful discussions; and Julie Suetterlin and Robin Roth for expert technical assistance. L.D.S. was the recipient of a Scholar Award in Molecular Parasitology from the Burroughs Wellcome Fund. D.S. is supported by Grant GM-067246 from the National Institutes of Health. The authors declare that they have no financial conflicts or competing interests.

REFERENCES

Allen, M. L., Dobrowolski, J. M., Muller, H., Sibley, L. D., and Mansour, T. E. (1997). Cloning and characterization of actin depolymerizing factor from *Toxoplasma gondii.* Mol. Biochem. Parasitol. *88*, 43–52.

Baldauf, S. L., Roger, A. J., Wenk-Siefert, I., and Doolittle, W. F. (2000). A kingdom-level phylogeny of eukaryotes based on combined protein data. Science *290*, 972–977.

Barragan, A., and Sibley, L. D. (2003). Migration of *Toxoplasma gondii* across biological barriers. Trends Microbiol. *11*, 426–430.

Bubb, M. R., Senderowicz, A.M.J., Sausville, E. A., Duncan, K.L.K., and Korn, E. D. (1994). Jasplakinolide, a cytotoxic natural product, induces actin polymerization and competitively inhibits the binding of phalloidin to F-actin. J. Biol. Chem. *269*, 14869–14871.

Bubb, M. R., Spector, I., Beyer, B. B., and Fosen, K. M. (2000). Effects of jasplakinolide on the kinetics of actin polymerization. J. Biol. Chem. *275*, 5163–5170.

Buscaglia, C. A., Coppens, I., Hol, W.G.J., and Nussenzweig, V. (2003). Site of interaction between aldolase and thrombospondin-related anonymous protein in *Plasmodium.* Mol. Biol. Cell *14*, 4947–4957.

Buzan, J., Du, J., Karpova, T., and Frieden, C. (1999). Histidine-tagged wild-type yeast actin: its properties and use in an approach for obtaining yeast actin mutants. Proc. Natl. Acad. Sci. USA *96*, 2823–2827.

Buzan, J., and Frieden, C. (1996). Yeast actin: polymerization kinetic studies of wild type and a poorly polymerizing mutant. Proc. Natl. Acad. Sci. USA *93*, 91–95.

Chen, X., Cook, R. K., and Rubenstein, P. A. (1993). Yeast actin with a mutation in the hydrophobic plug between subdomains 3 and 4 ($L_{266}D$) displays a cold-sensitive polymerization defect. J. Cell Biol. *123*, 1185–1195.

Chenna, R., Sugawara, H., Koike, T., Lopez, R., Gibson, T. J., Higgins, D. G., and Thompson, J. D. (2003). Multiple sequence alignment with the Clustal sequence series of programs. Nucleic Acids Res. *31*, 3497–3500.

Cooper, J. A., Buhle, E. L., Walker, S. B., Tsong, T. Y., and Pollard, T. D. (1983). Kinetic evidence for a monomer activation step in actin polymerization. Biochemistry *22*, 2193–2202.

Dobrowolski, J. M., Niesman, I. R., and Sibley, L. D. (1997). Actin in the parasite *Toxoplasma gondii* is encoded by a single copy gene, ACT1 and exists primarily in a globular form. Cell Motil. Cytoskelet. *37*, 253–262.

Dobrowolski, J. M., and Sibley, L. D. (1996). *Toxoplasma* invasion of mammalian cells is powered by the actin cytoskeleton of the parasite. Cell *84*, 933–939.

Doyle, T. C., Hansen, J. E., and Reisler, E. (2001). Tryptophan fluorescence of yeast actin resolved via conserved mutations. Biophys. J. *80*, 417–434.

Esue, O., Cordero, M., Wirts, D., and Tseng, Y. (2005). The assembly of MreB, a prokaryotic homolog of actin. J. Biol. Chem. 275. *280*, 2628–2635.

Frieden, C., Du, J., Schriefer, L., and Buzan, J. (2000). Purification and polymerization properties of two lethal yeast actin mutants. Biochem. Biophys. Res. Commun. *271*, 464–468.

Garner, E. C., Campbell, C. S., and Mullins, R. D. (2004). Dynamic instability in a DNA-segregating prokaryotic actin homolog. Science *306*, 1021–1025.

Gaskins, E., Gilk, S., DeVore, N., Mann, T., Ward, G. E., and Beckers, C. (2004). Identification of the membrane receptor of a class XIV myosin *Toxoplasma gondii.* J. Cell Biol. *165*, 383–393.

Håkansson, S., Morisaki, H., Heuser, J. E., and Sibley, L. D. (1999). Time-lapse video microscopy of gliding motility in *Toxoplasma gondii* reveals a novel, biphasic mechanism of cell locomotion. Mol. Biol. Cell *10*, 3539–3547.

Herm-Gotz, A., Weiss, S., Stratmann, R., Fujita-Becker, S., Ruff, C., Meyhofer, E., Soldati, T., Manstein, D. J., Geeves, M. A., and Soldati, D. (2002). *Toxoplasma gondii* myosin A and its light chain: a fast, single-headed, plus-end-directed motor. EMBO J. *21*, 2149–2158.

Higgins, D. G., Thompson, J. D., and Gibson, T. J. (1996). Using CLUSTAL for multiple sequence alignments. Methods Enzymol. *266*, 382–402.

Hirono, M., Kamagai, Y., Numata, O., and Watanabe, Y. (1989). Purification of *Tetrahymena* actin reveals some unusual properties. Proc. Natl. Acad. Sci. USA *86*, 75–79.

Hirono, M., Tanaka, R., and Watanabe, Y. (1990). *Tetrahymena* actin: copolymerization with skeletal muscle actin and interactions with muscle actin-binding proteins. J. Biochem. *107*, 3236

Humphrey, W., Dalke, A., and Schulten, K. (1996). VMD: visual modeling dynamics. Graph *14*, 33–38.

Jewett, T. J., and Sibley, L. D. (2003). Aldolase forms a bridge between cell surface adhesins and the actin cytoskeleton in apicomplexan parasites. Mol. Cell *11*, 885–894.

Kabsch, W., Mannherz, H. G., Suck, D., Pai, E. F., and Holmes, K. C. (1990). Atomic structure of actin: DNAseI complex. Nature *347*, 37–43.

Kuang, B., and Rubenstein, P. A. (1997). Beryllium fluoride and phalloidin restore polymerizability of a mutant yeast actin (V266G, L267G) with severely decreased hydrophobicity in a subdomain 3/4 loop. J. Biol. Chem. *272*, 1237–1247.

Mead, P. S., Slutsker, L., Dietz, V., McCaig, L. F., Bresee, J. S., Shapiro, C., Griffin, P. M., and Tauxe, R. V. (1999). Food-related illness and death in the United States. Emerg. Infect. Dis. *5*, 607–625.

Meissner, M., Schluter, D., and Soldati, D. (2002). Role of *Toxoplasma gondii* myosin A in powering parasite gliding and host cell invasion. Science *298*, 837–840.

Morrissette, N. S., and Sibley, L. D. (2002). Cytoskeleton of apicomplexan parasites. Microbiol. Mol. Biol. Rev. *66*, 21–38.

Nishida, E., and Sakai, H. (1983). Kinetic analysis of actin polymerization. J. Biochem. *93*, 1011–1020.

Orlova, A., Shvetsov, A., Galkin, V. E., Kudryashov, D. S., Rubenstein, P. A., Egelman, E. H., and Reisler, E. (2004). Actin-destabilizing factors disrupt filaments by means of a time reversal of polymerization. Proc. Nat. Acad. Sci. USA *101*, 17664–17668.

Otterbein, L. R., Graceffa, P., and Dominguez, R. (2001). The crystal structure of uncomplexed actin in the ADP bound state. Science *293*, 708–711.

Pardee, J. D., and Spudich, J. A. (1982). Purification of muscle actin. Methods Cell Biol. *24*, 271–289.

Pollard, T. D. (1984). Polymerization of ADP-actin. J. Cell Biol. *99*, 769–777.

Pollard, T. D., Blanchoin, L., and Mullins, R. D. (2000). Molecular mechanisms controlling actin filament dynamics in nonmuscle cells. Annu. Rev. Biophys. Biomol. Struct. *29*, 545–576.

Pollard, T. D., and Borisy, G. G. (2003). Cellular motility driven by assembly and disassembly of actin filaments. Cell *112*, 453–465.

Poupel, O., and Tardieux, I. (1999). *Toxoplasma gondii* motility and host cell invasiveness are drastically impaired by jasplakinolide, a cyclic peptide stabilizing F-actin. Microbes Infect. *1*, 653–662.

Schmitz, S., Grainger, M., Howell, S. A., Calder, L. J., Gaeb, M., Pinder, J. C., Holder, A. A., and Veigel, C. (2005). Malaria parasite actin filaments are very short. J. Mol. Biol. *349*, 113–125.

Schoenenberger, C. A., Bischler, N., Fahrenkrog, B., and Aebi, U. (2002). Actin's propensity for dynamic filament patterning. FEBS Lett. *529*, 27–33.

Schuler, H., Mueller, A. K., and Matuschewski, K. (2005). Unusual properties of *Plasmodium falciparum* actin: new insights into microfilament dynamics of apicomplexan parasites. FEBS Lett. *579*, 655–660.

Shaw, M. K., and Tilney, L. G. (1999). Induction of an acrosomal process in *Toxoplasma gondii*: visualization of actin filaments in a protozoan parasite. Proc. Natl. Acad. Sci. USA *96*, 9095–9099.

Sibley, L. D. (2004). Invasion strategies of intracellular parasites. Science *304*, 248–253.

Sultan, A. A., Thathy, V., Frevert, U., Robson, K.J.H., Crisanti, A., Nussenzweig, V., Nussenzweig, R. S., and Menard, R. (1997). TRAP is necessary for gliding motility and infectivity of *Plasmodium* sporozoites. Cell *90*, 511–522.

Swofford, D. L. (1998). PAUP Phylogenetic Analysis Using Parsimony and Other Methods, Sunderland, MA: Sinauer Associates.

Tobacman, L., and Korn, E. D. (1983). The kinetics of actin nucleation and polymerization. J. Biol. Chem. 275. *258*, 3207–3214.

Wetzel, D. M., Håkansson, S., Hu, K., Roos, D. S., and Sibley, L. D. (2003). Actin filament polymerization regulates gliding motility by apicomplexan parasites. Mol. Biol. Cell *14*, 396–406.